Research Article | Vol. 28, No. 2 / 20 January 2020 / Optics Express 1076
Optics EXPRESS

# Polarization dependent cladding modes coupling and spectral analyses of excessively tilted fiber grating

FANGCHENG SHEN,[1,2] KAIMING ZHOU,[3] CHANGLE WANG,[3] HAIMING JIANG,[1,2] DI PENG,[1,2] HONGYAN XIA,[1,2] KANG XIE,[1,2,*] AND LIN ZHANG[3]

[1]*Dongyuan Synergy Innovation Institute for Modern Industries of GDUT, Guangdong University of Technology, Guangzhou 510006, China*
[2]*School of Electromechanical Engineering, Guangdong University of Technology, Guangzhou 510006, China*
[3]*Institute of Photonic and Technologies, Aston University, Birmingham B4 7ET, UK*
[*]*kangxie@gdut.edu.cn*

**Abstract:** We report on the detailed analyses of mode coupling from fiber core to cladding in excessively tilted fiber gratings (ETFGs). Cladding modes responsible for the typical dual peak pairs in the transmission spectrum of ETFGs are identified with phase matching condition, which suggests two set of dual peak pairs generated from coupling to cladding modes with even and odd azimuthal order. The polarization dependence of those dual peak pairs are also investigated by calculating the coupling coefficients of cladding modes for two orthogonal polarizations. With the calculated coupling coefficients, the measured polarization dependent spectra can be reproduced numerically.



## 1. Introduction

Refractive index (RI) is an important parameter in bio/chemical applications where the interaction process can be monitored by RI variation. Optical fiber grating (OFG) sensors have the advantages of compactness, low insertion loss and most importantly, strong tolerance of chemical corrosion that make them promising candidate for RI sensing and the related applications. For OFGs in standard single mode fiber (SSMF), there are mainly two ways to make them sensitive to surrounding RI change: one is through the modification of fiber structure to expose fiber core to surrounding material [1,2], which usually involves the use of hazardous hydrofluoric acid and can degrade the mechanical strength of the fiber; The other is the excitation of cladding modes that can directly interact with surrounding environment. To date, there are mainly three kinds of OFGs that allow coupling from core mode to cladding modes, e.g., tilted fiber Bragg gratings (TFBGs), excessively tilted fiber gratings (ETFGs), and long period fiber gratings (LPFGs) [3–5]. However, the RI sensitivities of TFBGs are relatively low [6], while LPFGs suffer from strong cross-sensitivity to surrounding perturbations, such as temperature [7]. Moreover, the large bandwidths of LPFGs limit their RI sensing resolution [8].

The excessively tilted fiber gratings (ETFGs), which were first proposed and demonstrated by K. Zhou et al in 2006 [4], are a relatively new kind of fiber gratings characterized by large tilt angle $\theta$= ~81 ° (Fig. 1). In ETFGs, core propagating light is coupled to co-propagating cladding modes, which decay rapidly as they propagate along the fiber axis [5], leaving several attenuation bands in the transmission spectrum. Since proposed, ETFGs have attracted considerable attention in RI sensing applications due to their advantages of high RI sensitivities, narrow bandwidth and low thermal cross-sensitivity [9,10], and many bio-chemical sensors based on ETFGs have also been reported [11–14]. Apart from great potential in sensing applications, the unique polarization

#382528 https://doi.org/10.1364/OE.382528
Journal © 2020 Received 8 Nov 2019; revised 25 Dec 2019; accepted 29 Dec 2019; published 6 Jan 2020

Optics EXPRESS

dependent dual peak pairs of ETFGs also make them promising in fiber laser applications, and several wavelength switchable laser schemes have been implemented [15,16].

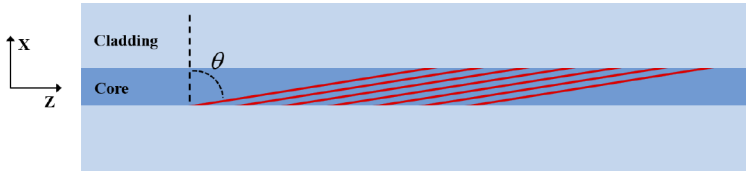


**Fig. 1.** Schematic of excessively tilted fiber grating.

In spite of many experimental works on ETFGs reported, theoretical analyses about ETFGs, especially about the polarization dependent dual peaks, are rarely testified. In 2016, Z. Yan et al gave detailed theoretical and experimental analyses of ETFGs [17], and concluded that the polarization dependent dual peaks are generated from coupling to $TM_{0m}$ and $TE_{0m}$ cladding modes, but the theoretically predicted number of dual peak pairs (5 pairs) mismatches the experimental results (7 pairs).

In this work, we analyze the polarization dependent cladding mode coupling characteristics in ETFGs, and reveal that apart from $TM_{0m}$ and $TE_{0m}$ cladding modes, HE/EH hybrid cladding modes also play an important role in the generation of polarization dependent dual peak pairs (detailed definition and classification of fiber cladding modes can be found in [18,19]). The coupling coefficients of those modes depend strongly on the input polarization status, and a good agreement between theoretical and experimental results is achieved when HE/EH cladding modes are taken into account. The mismatch of peak pair numbers in [17] can also be explained with our finding.

## 2. Fabrication and spectra of ETFG

To fabricate the ETFGs, commercial SSMF (Corning SM 28) was hydrogen-loaded first to enhance its UV photosensitivity. A frequency-doubled $Ar^+$ laser with a central wavelength of 244 nm was used for the inscription. The grating period was determined by a custom-designed amplitude mask, which has a period of 6.6 μm. During the fabrication, the amplitude mask was rotated by ~76.5 ° relative to the fiber axis to introduce grating structure with a tilt angle of ~81° (±1° deviation) [17]. The fabricated grating with a total length of 12 mm was annealed at 80°C for 48 h to stabilize the UV-induced RI modification.

Figure 2(a) shows the transmission spectrum of the fabricated ETFG. During the measurement, the fiber following the grating is kept long enough to fully attenuate the exited cladding modes. In Fig. 2(a), 5 dual peak pairs can be observed in the wavelength region from 1.4 to 1.7 μm. The quasi-periodic ripples in the spectrum are believed to result from the interference of core mode with light scattered into fiber cladding [20]. The peak pairs are label as P1-5 for the convenience of following analyses. We can see that for each peak pair, the peak on the right side (indicated by magenta dashed line) is much stronger than the one on the left side (indicated by blue dashed line), suggesting that the light source used for measurement may be partially polarized, as the peak pairs have polarization dependent strength [4]. Those peak pairs are fully distinguishable when polarized light are used, as shown in Fig. 2(b), where a polarizer followed by a polarization controller was used to control the polarization of input light. In Fig. 2(b), P polarization refers to polarization parallel to grating tilt plane (X-Z plane in Fig. 1), while S polarization is vertical to grating tilt plane. Strong polarization dependent coupling strength can be observed in Fig. 2(b). The working principle of those polarization dual peak pairs will be investigated in the following section.

Optics EXPRESS

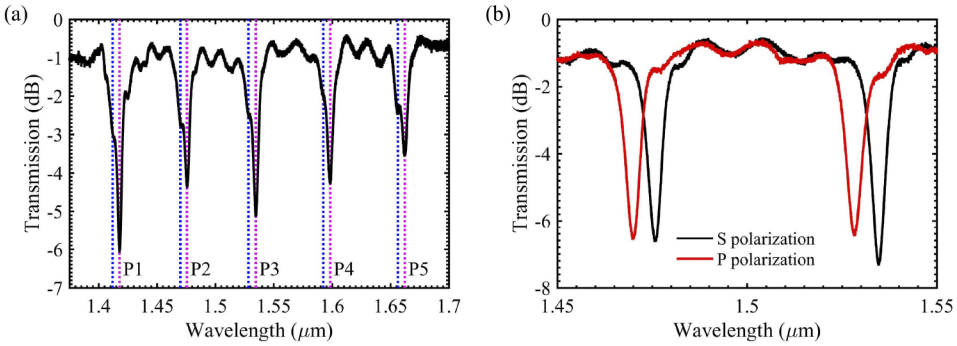


**Fig. 2.** Transmission spectra of the fabricated ETFG measured with (a) un-polarized light and (b) polarized light with different polarization as the input.

## 3. Theoretical analyses and discussion

### 3.1. Resonant wavelengths

In an ETFG, energy of core mode is coupled to co-propagating cladding modes at wavelengths determined by phase matching condition:

$$\lambda = (neff^{co}(\lambda) - neff^{cl}_{l,m}(\lambda)) * \Lambda \tag{1}$$

where $\lambda$ is the resonant wavelength; $neff^{co}(\lambda)$ and $neff^{cl}_{l,m}(\lambda)$ are the effective RI of core mode and cladding mode at $\lambda$ respectively; $l$ and $m$ represent the azimuthal and radial order of the cladding modes, and $\Lambda$ is the grating period along fiber axis, which can be calculated from grating tilt angle $\theta$ and the period of the amplitude mask $\Lambda_{AM}$ by:

$$\Lambda = \frac{\Lambda_{AM}}{\cos\theta} \tag{2}$$

The phase matching condition can be used to predict the grating resonant wavelengths in advance, and identify the participating modes for resonances in the measured spectrum. To get the relationship between the grating period and resonant wavelengths, the effective RI of the core and cladding modes need to be calculated first, which can be obtained by solving the dispersion relation of three-layer step-index fiber [19,21,22]. The solutions of the equation that describes the dispersion relation of fiber cladding modes are indicated by two integers: an azimuthal order $l$ that describes the azimuthal variation of the mode field, and a radial order $m$ that is related to the radial distribution of certain cladding mode. For a given azimuthal order $l$, the radial order $m$ numbers all solutions, starting with $m = 1$ for the solution with the highest effective RI [19,23], followed by m = 2, 3, 4. . . with decreasing mode effective RI. In our calculation, the fiber core and cladding radius are set to be 4.05 μm and 62.5 μm respectively; the RIs of fiber core and cladding are calculated by Sellmeier equation, with core and cladding composition set to be 3.315 m% $GeO_2$ and pure silica, and the fiber is surrounded by air with $n_{air} = 1$; the UV induced RI modulation in the core is averaged by: $n_{new} = n_{core} + dn/2$, where $n_{core}$ is the un-modulated core RI calculated by Sellmeier equation, and UV induced RI modulation $dn$ is uniform along the grating with a value of $5.5\times10^{-4}$.

The calculated phase matching curves for cladding modes with azimuthal order up to 5 are shown in Fig. 3, where the resonant wavelengths measured from Fig. 2(a) are also indicated by vertical dashed lines. The two horizontal dashed lines represent the grating period calculated with a tilt angle of 81° (green) and 79.4862° (purple). The intersections between the horizontal line and phase matching curves indicate the predicted resonant wavelengths of grating with

Optics EXPRESS

the corresponding period. For resonant wavelengths of a grating whose period is known, the corresponding phase matching curve in Fig. 3 can be identified, and thus the radial order. We can see from Fig. 3 that the resonant wavelengths predicted by purple line allow a good agreement with experimental ones, suggesting the actual grating tilt angle is ~79.4862°. It can also be observed from Fig. 3 that: (i) HE (TE) and EH (TM) cladding modes with even (odd) azimuthal order degenerate, e.g., $TE_{0,m}$, $HE_{2,m}$, and $HE_{4,m}$ modes have almost the same resonant wavelength, as indicated by the vertical blue line of P2 and P4; (ii) the HE (TE) and EH (TM) modes with the same azimuthal order are nearly but not degenerate, e.g., $TE_{0m}$ and $TM_{0m}$ modes give two closely separated resonances, and that's why the resonances in the transmission spectrum of ETFGs usually appear in pairs; (iii) there are two sets of peak pairs, with one generated from coupling to cladding modes with even azimuthal order (P2 and P4) and the other from odd azimuthal order (P1, P3, and P5). The two sets of peak pairs appear alternatively in the transmission spectrum of ETFG. This finding explains the mismatch between the theoretically predicted number of dual peak pairs and experimental measured number in [17], where cladding modes with azimuthal order $l \geq 1$ are not considered.

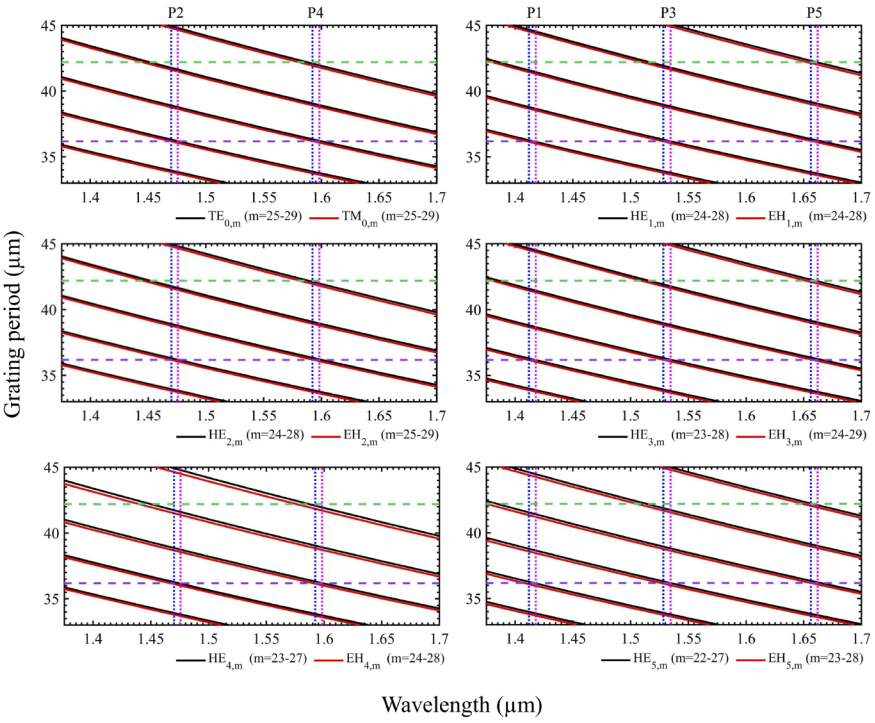


**Fig. 3.** Phase matching curves for cladding modes with azimuthal order up to 5. The range of radial order $m$ is given in the legend, which increases sequentially from the top right to the bottom left. The two horizontal dashed lines indicate the grating period calculated with a tilt angle of 81° (green) and 79.4862° (purple). The vertical lines represent experimentally measured resonant wavelengths.

### *3.2. Polarization dependent coupling coefficient and spectral analyses*

Note that since modes with even (odd) azimuthal order degenerate, each resonance in the transmission spectrum corresponds to coupling to several cladding modes. Such degeneration can be beneficial if we focus on predicting the resonant wavelengths, as the degenerate modes have almost the same resonant wavelengths that can be determined with one phase matching

Optics EXPRESS

curve. However, to evaluate the contribution of each cladding mode for certain resonance, the coupling coefficients need to be calculated. The coupling coefficient of tilted fiber grating can be written as follows [24]:

$$\kappa_{l,m}^{co} = \frac{\pi n_1 \Delta n}{4\lambda Z_0} \int_0^{2\pi} \int_0^{a_1} (E_{co} \cdot E_{l,m}^*) \cos(2K_g r \cos\phi \sin\theta) r dr d\phi \tag{3}$$

where the free space impedance $Z_0 = 377\Omega$; the grating wave-vector $K_g = 2\pi/(\Lambda_{AM}/\cos\theta)$;$E_{co}$ and $E_{l,m}$ are the electric fields of involved core and cladding modes. The integration is limited to core region because only the core region is photosensitive to UV inscription.

During the calculation, $HE_{11}$ core modes with orthogonal polarizations (S and P as defined in Section 2) are used as the input to illustrate the polarization dependent coupling in ETFGs. Any other polarization states can be decomposed as a superposition of those two polarizations. The grating tilt angle is set to be 79.4862°, corresponding to an axial grating period of 36.1699 μm, as indicated by the purple horizontal line in Fig. 3. This tilt angle differs from the experimental one, because in our experiment, the tilt angle was manually controlled with a goniometer, and it is difficult to set the tilt angle exactly and may introduce a ~ ±1° deviation.

The calculated coupling coefficients for cladding modes with different azimuthal and radial order are shown in Fig. 4, where coupling coefficients for S and P polarizations are represented with black and red color respectively. Note that in tilted fiber grating, coupling between different polarizations is forbidden, and for TE and TM modes, only one polarization is considered, because coupling from the other polarization is not allowed [25]. Coupling coefficients for cladding modes with azimuthal order $l$>5 are one order of magnitude smaller, and are not shown here. From Fig. 4, we can clearly see that coupling to HE (TE) modes is much stronger for S polarization, while for EH (TM) modes, coupling from P polarizations dominates. This polarization dependent coupling strength, combined with the characteristics of resonant wavelengths given in Section 3.1, accounts for the polarization dependent dual peak pairs in Fig. 2(b).

To help understand the trend of the coupling coefficients in Fig. 4, several exemplary cladding mode fields are presented in Fig. 5, where the core-cladding boundary is indicated by the black circles. The radial order is set to be 25, since the cladding modes responsible for the experimental transmission spectra have radial order close to this value, as shown in Fig. 3. Note that in Fig. 5, the notation "even" and "odd" refer to the two polarization degenerate counterpart of hybrid modes [26]. We can see from the vector field in Fig. 5 that, with relatively high radial order, HE modes are TE like, while EH-modes are TM-like, especially for HE/EH modes with azimuthal order $l = 1$. This observation agrees with previous reports [19,25]. Due to the fact that TE and TM modes only allow coupling from one polarization [19,25], those TE or TM-like hybrid modes also exhibit strong polarization dependent coupling, as depicted in Fig. 4. The fields of $HE/EH_{4,\,25}$ in Fig. 5, where the vector become messy in the dark area of the intensity field, show that cladding modes with high azimuthal order are less TE/TM-like, and consequently the polarization dependence degenerates with the increment of azimuthal order (Fig. 4). Moreover, $HE/EH_{1,\,25}$ mode fields in Fig. 5 have a maximum in the core center, where fundamental core mode also has the maximum intensity, so the interaction between them is strong, thus allowing a high coupling efficiency; while for $HE/EH_{4,\,25}$ modes, the energy within the core resides mainly near the core-cladding boundary, where fundamental core mode intensity becomes weak, resulting in a weak interaction and consequently, low coupling efficiency.

The calculated coupling coefficients are substituted into coupled mode equations to get the transmission spectra. Figure 6 shows the calculated and measured transmission spectra for S and P polarizations, where a background loss of 0.98 dB was introduced for calculated spectra to account for the experimental loss. Cladding modes with azimuthal order up to 10 were taken into account during the calculation. We can see from Fig. 6 that, both of them exhibit strong

Optics EXPRESS

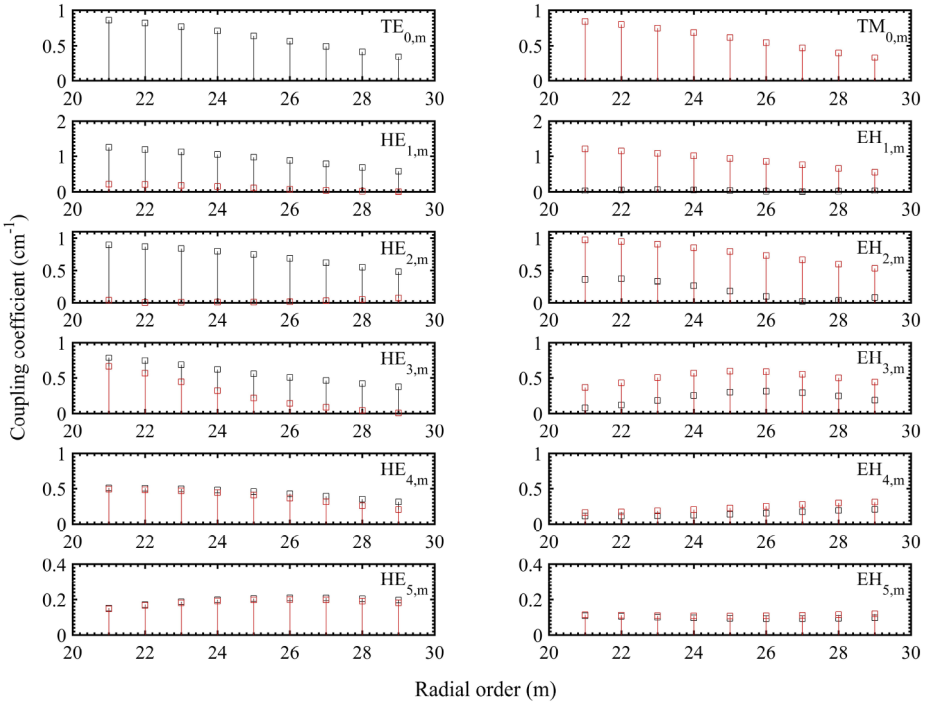


**Fig. 4.** Calculated coupling coefficients for different cladding modes. The black color represents coupling from S polarization core mode and red for P polarization.

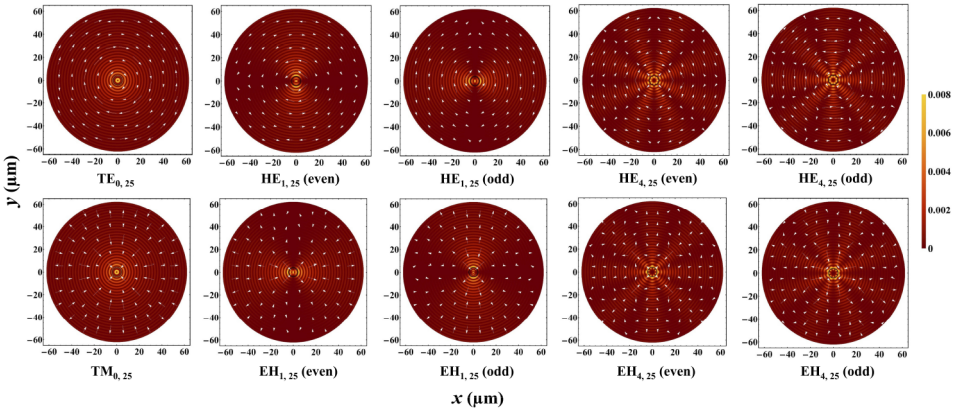


**Fig. 5.** Exemplary intensity field of TE, TM and HE/EH mode. The white arrows depict the electric field. The black circles indicate the core-cladding boundary.

polarization dependence, and a close agreement is achieved between the calculated and measured spectra for P2 and P3, especially their resonant wavelengths. For other peak pairs, the maximum wavelength deviation between the calculated and measured resonant wavelengths is ~5 nm, which is believed to be acceptable considering the wide wavelength range of more than 350 nm. The difference in the strength of the resonant peaks can be attributed to the fact that the exact fiber parameters, such as core composition, are unknown. Moreover, the background ripples in the measured transmission spectra can also lead to some mismatch in strength.

Optics EXPRESS

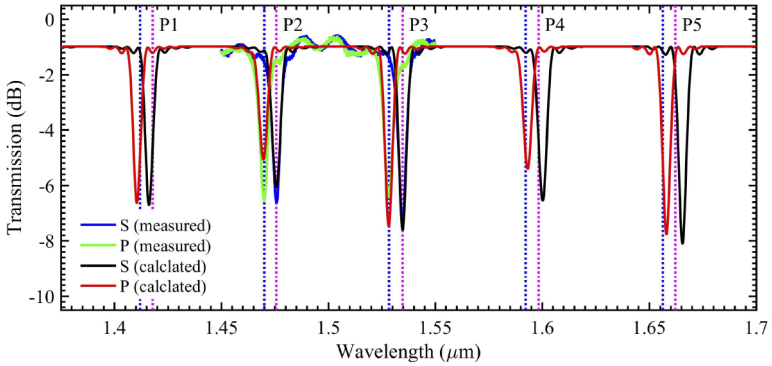


**Fig. 6.** Calculated and measured transmission spectra for S and P polarizations. The resonant wavelengths labeled in Fig. 2(a) are indicated by vertical lines.

## 4. Conclusion

In summary, we have investigated the polarization dependent cladding modes coupling behavior of ETFGs. Based on the phase matching condition and taking account of cladding modes with high azimuthal order, we identified the cladding modes that are responsible for the generation of dual peak pairs, and the theoretically predicted resonant wavelengths agree well with the experimentally measured ones.

Further calculation of the coupling coefficients for two orthogonal polarizations suggests that, coupling to HE (TE) modes is much stronger for S polarization, while for EH (TM) modes, coupling from P polarizations dominates. The polarization dependent dual peak pairs in ETFGs can be well explained by the polarization dependent coupling behavior at nearly degenerate wavelengths, and a good agreement between calculated and measured spectra is achieved for two polarizations. The results presented in this work can deepen the understanding of the working principle of ETFGs, and serve as a foundation for the design of ETFGs and the related applications.

## Funding

National Natural Science Foundation of China (11574070, 11874126, 51803037, 61805046); Leading Talents Program of Guangdong Province.

## References

1. S. G. Kilic, Y. Zhu, Q. Sheng, M. N. Inci, and M. Han, "Refractometer With Etched Chirped Fiber Bragg Grating Fabry–Perot Interferometer in Multicore Fiber," IEEE Photonics Technol. Lett. **31**(8), 575–578 (2019).
2. K. Zhou, Y. Lai, X. Chen, K. Sugden, L. Zhang, and I. Bennion, "A refractometer based on a micro-slot in a fiber Bragg grating formed by chemically assisted femtosecond laser processing," Opt. Express **15**(24), 15848–15853 (2007).
3. T. Erdogan and J. E. Sipe, "Tilted fiber phase gratings," J. Opt. Soc. Am. A **13**(2), 296–313 (1996).
4. K. Zhou, L. Zhang, X. Chen, and I. Bennion, "Optic sensors of high refractive-index responsivity and low thermal cross sensitivity that use fiber Bragg gratings of > 80 tilted structures," Opt. Lett. **31**(9), 1193–1195 (2006).
5. A. M. Vengsarkar, P. J. Lemaire, J. B. Judkins, V. Bhatia, T. Erdogan, and J. E. Sipe, "Long-period fiber gratings as band-rejection filters," J. Lightwave Technol. **14**(1), 58–65 (1996).
6. C. F. Chan, C. Chen, A. Jafari, A. Laronche, D. J. Thomson, and J. Albert, "Optical fiber refractometer using narrowband cladding-mode resonance shifts," Appl. Opt. **46**(7), 1142–1149 (2007).
7. V. Bhatia and A. M. Vengsarkar, "Optical fiber long-period grating sensors," Opt. Lett. **21**(9), 692–694 (1996).
8. J. Albert, L. Y. Shao, and C. Caucheteur, "Tilted fiber Bragg grating sensors," Laser Photonics Rev. **7**(1), 83–108 (2013).

Optics EXPRESS


9. Z. Yan, Z. Sun, K. Zhou, B. Luo, J. Li, H. Wang, Y. Wang, W. Zhao, and L. Zhang, "Numerical and experimental analysis of sensitivity-enhanced RI sensor based on Ex-TFG in thin cladding fiber," J. Lightwave Technol. **33**(14), 3023–3027 (2015).
10. Z. Yan, Q. Sun, C. Wang, Z. Sun, C. Mou, K. Zhou, D. Liu, and L. Zhang, "Refractive index and temperature sensitivity characterization of excessively tilted fiber grating," Opt. Express **25**(4), 3336–3346 (2017).
11. B. Luo, Z. Yan, Z. Sun, J. Li, and L. Zhang, "Novel glucose sensor based on enzyme-immobilized 81° tilted fiber grating," Opt. Express **22**(25), 30571–30578 (2014).
12. B. Luo, Y. Xu, S. Wu, M. Zhao, P. Jiang, S. Shi, Z. Zhang, Y. Wang, L. Wang, and Y. Liu, "A novel immunosensor based on excessively tilted fiber grating coated with gold nanospheres improves the detection limit of Newcastle disease virus," Biosens. Bioelectron. **100**, 169–175 (2018).
13. B. Jiang, K. Zhou, C. Wang, Q. Sun, G. Yin, Z. Tai, K. Wilson, J. Zhao, and L. Zhang, "Label-free glucose biosensor based on enzymatic graphene oxide-functionalized tilted fiber grating," Sens. Actuators, B **254**, 1033–1039 (2018).
14. B. Jiang, Z. Bi, Z. Hao, Q. Yuan, D. Feng, K. Zhou, L. Zhang, X. Gan, and J. Zhao, "Graphene oxide-deposited tilted fiber grating for ultrafast humidity sensing and human breath monitoring," Sens. Actuators, B **293**, 336–341 (2019).
15. C. Mou, P. Saffari, H. Fu, K. Zhou, L. Zhang, and I. Bennion, "Single-and dual-wavelength switchable erbium-doped fiber ring laser based on intracavity polarization selective tilted fiber gratings," Appl. Opt. **48**(18), 3455–3459 (2009).
16. Z. Zhang, C. Mou, Z. Yan, Y. Wang, K. Zhou, and L. Zhang, "Switchable dual-wavelength Q-switched and mode-locked fiber lasers using a large-angle tilted fiber grating," Opt. Express **23**(2), 1353–1360 (2015).
17. Z. Yan, H. Wang, C. Wang, Z. Sun, G. Yin, K. Zhou, Y. Wang, W. Zhao, and L. Zhang, "Theoretical and experimental analysis of excessively tilted fiber gratings," Opt. Express **24**(11), 12107–12115 (2016).
18. J. U. Thomas, N. Jovanovic, R. G. Becker, G. D. Marshall, M. J. Withford, A. Tünnermann, S. Nolte, and M. J. Steel, "Cladding mode coupling in highly localized fiber Bragg gratings: modal properties and transmission spectra," Opt. Express **19**(1), 325–341 (2011).
19. J. U. Thomas, N. Jovanovic, R. G. Krämer, G. D. Marshall, M. J. Withford, A. Tünnermann, S. Nolte, and M. J. Steel, "Cladding mode coupling in highly localized fiber Bragg gratings II: complete vectorial analysis," Opt. Express **20**(19), 21434–21449 (2012).
20. P. Chen, X. Shu, F. Shen, and H. Cao, "Sensitive refractive index sensor based on an assembly-free fiber multi-mode interferometer fabricated by femtosecond laser," Opt. Express **25**(24), 29896–29905 (2017).
21. T. Erdogan, "Cladding-mode resonances in short-and long-period fiber grating filters," J. Opt. Soc. Am. A **14**(8), 1760–1773 (1997).
22. T. Erdogan, "Cladding-mode resonances in short-and long-period fiber grating filters: errata," J. Opt. Soc. Am. A **17**(11), 2113 (2000).
23. B. E. A. Saleh and M. C. Teich, "Fundamentals of photonics," Wiley, 278–281 (1991).
24. K. Lee and T. Erdogan, "Fiber mode coupling in transmissive and reflective tilted fiber gratings," Appl. Opt. **39**(9), 1394–1404 (2000).
25. M. Z. Alam and J. Albert, "Selective excitation of radially and azimuthally polarized optical fiber cladding modes," J. Lightwave Technol. **31**(19), 3167–3175 (2013).
26. A. Snyder and J. Love, "Optical Waveguide Theory," Springer-Verlag, New York, NY, USA, 249 (1983).